Design of Single Gold Atoms on Nitrogen-Doped Carbon for Molecular Recognition in Alkyne Semi-Hydrogenation

Ronghe Lin[+], Davide Albani[+], Edvin Fako, Selina K. Kaiser, Olga V. Safonova, Núria López,* and Javier Pérez-Ramírez*

Abstract: *Single-atom heterogeneous catalysts with well-defined architectures are promising for deriving structure–performance relationships, but the challenge lies in finely tuning the structural and electronic properties of the metal. To tackle this point, a new approach based on the surface diffusion of gold atoms on different cavities of N-doped carbon is presented. By controlling the activation temperature, the coordination neighbors (Cl, O, N) and the oxidation state of the metal can be tailored. Semi-hydrogenation of various alkynes on the single-atom gold catalysts displays substrate-dependent catalytic responses; structure insensitive for alkynols with γ-OH and unfunctionalized alkynes, and sensitive for alkynols with α-OH. Density functional theory links the sensitivity for alkynols to the strong interaction between the substrate and specific gold-cavity ensembles, mimicking a molecular recognition pattern that allows to identify the cavity site and to enhance the catalytic activity.*

Identifying the structure of the active site of a catalyst is pivotal for rational design. While the architecture of homogeneous systems can be easily characterized, the analogue in heterogeneous catalysis remains very challenging due to the inherent material complexity, even though advanced in situ and operando techniques are nowadays widely available. For this reason, synthesis of heterogeneous metal catalysts with well-defined active ensembles to mimic organometallic complexes is regarded as an elegant approach, which might not only enable selective transformations,[1] but exquisitely lead to the establishment of new structure–performance relation-

ships.[2] Single-atom heterogeneous catalysts (SAHCs), a class of burgeoning materials with diverse applications in chemical transformation[2a,c] and energy conversion,[3] can be envisaged as the missing link between homogeneous and heterogeneous systems owing to the intrinsic cationic nature and well isolation of the single metal atoms entrapped in a solid material acting as ligand. To overcome their tendency of metal agglomeration, extensive efforts have been devoted to developing effective synthetic strategies via either introducing suitable anchoring sites or creating strong metal-support interactions, as recently well documented for a wide range of transition metals on different hosts.[4] Despite being successfully applied in different reactions, still the rational design of SAHCs for targeted applications is at the initial stage. Consequently, this leads to a knowledge gap whether concepts belonging to homogeneous catalysts could be transposed to the heterogeneous counterparts.

Catalysis by gold has witnessed exceptional growth in diverse fields since this metal is both effective as a homogeneous or a heterogeneous catalyst.[5] In view of the nowadays growing importance of gold nanoparticles and single atoms in hydrogenation,[6] oxidation,[7] water-gas shift,[2a,b] and hydrochlorination,[8] an in depth study on the precise control over the metal oxidation state and coordination sphere of single gold atoms using nitrogen-doped carbon (NC) is targeted. This is achieved by inducing surface diffusion of metal atoms on the diverse anchoring sites of the host, which leads to the creation of a series of single-atom gold ensembles with well-defined structures and electronic properties. Inspired by the opposite origins for supported gold nanoparticles and homogeneous gold complexes governing the selective activation of alkynes (a phenomenon known as alkynophilicity[9]), the Au SAHCs with precise architectures are assessed in the semi-hydrogenation of alkynes to establish catalyst design rules.

Gold was deposited via incipient wetness impregnation of $HAuCl_4$ in an aqua regia solution either on sulfur-free polyaniline-derived high N-content NC (ca. 10 wt %)[10] or activated carbon (AC, as a reference) followed by thermal activation at different atmospheres and temperatures (413–1073 K) for 16 h (Figure 1, see the Supporting Information for more details). The temperature-dependent evolution of Au particle size for both series was followed by X-ray diffraction patterns (XRD). Apart from showing the amorphous nature of the NC support and the absence of any Au related diffraction patterns on Au/NC-*T* (where *T* stands for the treatment temperature applied), it reveals the characteristic peaks of the Au(111) facet at *T* ≥ 573 K on the AC reference (Figure S1). The diverging evolution of the gold atoms on both carriers was further analyzed by combining high-angle

[*] Dr. R. Lin,[+] D. Albani,[+] S. K. Kaiser, Prof. J. Pérez-Ramírez
Institute for Chemical and Bioengineering
Department of Chemistry and Applied Biosciences
ETH Zurich
Vladimir-Prelog-Weg 1, 8093 Zurich (Switzerland)
E-mail: jpr@chem.ethz.ch

E. Fako, Prof. N. López
Institute of Chemical Research of Catalonia (ICIQ)
The Barcelona Institute of Science and Technology
Av. Països Catalans 16, 43007 Tarragona (Spain)
E-mail: nlopez@iciq.es

Dr. O. V. Safonova
Paul Scherrer Institute
5232 Villigen PSI (Switzerland)

[+] These authors contributed equally to this work.

Supporting information (catalyst preparation, characterization, and evaluation as well as computational methods) and the ORCID identification number(s) for the author(s) of this article can be found under:
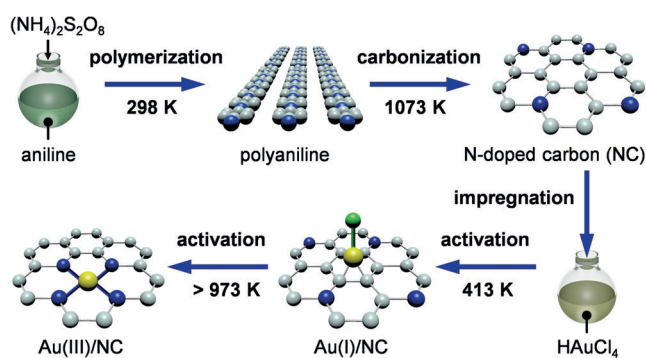https://doi.org/10.1002/anie.201805820.

Figure 1. Synthetic steps involved in the preparation of nitrogen-doped carbon (NC) with a high density of electron-rich cavities: oxidative polymerization of aniline with ammonium persulfate to polyaniline and subsequent carbonization of the polymer at 1073 K, and the subsequent preparation of supported single-atom gold catalysts via incipient wetness impregnation of NC with $HAuCl_4$ in aqua regia solution, followed by thermal activation step in static air ($\leq$ 473 K) or flowing N_2 (> 473 K) for 16 h. Au yellow, C gray, N blue, and Cl green.

annular dark-field scanning transmission electron microscope (HAADF-STEM, Figure 2a,b, Figures S2 and S3 in the Supporting Information) and extended X-ray absorption fine structure spectroscopy (EXAFS, Figure 2e), confirming that the gold species are present as single atoms on the NC carrier even up to 1073 K. In stark contrast, single Au atoms hosted on the AC are stable only at 413 K and dramatic agglomeration occurs readily at $T \geq$ 573 K, featuring scattering peaks assigned to the Au-Au bonds in the Au/AC-673 sample (Figure 2e) and very wide particle size distribution (Figure S4).

To assess the individual roles of aqua regia and the N sites, an additional Au/NC-413(H_2O) sample was prepared using deionized water as solvent. The XRD patterns of the sample dried at 413 K show clear reflections of metallic gold (Figure S1). This result together with the diverging evolution of gold on both carbon hosts highlights the important roles of the solvent and N dopant in stabilizing single-gold atoms on the carbon host (details are given in the Supporting Information).

To reveal the nature of the gold species on Au/NC-*T* and Au/AC-*T*, X-ray photoelectron spectroscopy (XPS) was conducted. Interestingly, for the NC series the Au 4f core level spectra steadily shift to higher binding energy (BE) upon increasing activation temperature (Figure 2c). This behavior is not observed on the AC references, as evidenced from the similar Au $4f_{7/2}$ peaks at BE = 84.2 eV for metallic Au on both Au/AC-413 and Au/AC-673. Detailed XPS fitting for Au/NC samples indicates that the low-temperature sample contains predominantly Au species at BE = 84.2 eV which decrease in population with increasing temperature, while the contents of Au^+ (BE = 85.0 eV) and Au^{3+} (BE = 87.0 eV) increase. At T = 1073 K, Au^{3+} was the only species stable at such a high temperature. Thus, the well-behaved temperature dependency of the Au oxidation state enables ad hoc tuning of the Au/NC system for targeted applications.

The precise assignment of the low BE peak should be done with caution as gold chloride species are highly light-sensitive and can be reduced to Au^0 during XPS measurement.[11] To complement the XPS findings, X-ray absorption near edge spectroscopy (XANES) was applied as a non-destructive technique for these sensitive materials. Figure 2d presents the XANES spectra of relevant samples together with reference gold standards. For the two extreme Au/NC samples (Au/NC-413 and Au/NC-1073) and Au/AC-413, a clear white line peaked at approximately 11 919–11 920 eV was observed. Besides, the absorption threshold of gold, obtained from the first derivative of the normalized absorption curves (Figure S5), shows a clear shift to higher energy for the Au/NC samples as compared to the Au foil, indicating the cationic gold speciation in these materials.[12] On the contrary, the Au/AC-673, containing mainly Au nanoparticles, did not show these features, albeit sharing a similar Au 4f XPS spectrum. Still, differences between Au/NC-413 and Au/NC-1073 can be distinguished in their normalized white line intensity (0.73 vs. 1.15), a feature corresponding to d-electron occupancy.[8] By comparing these values with those of gold references, we can thus confirm that Au^+ and Au^{3+} are the major species in Au/NC-413 and Au/NC-1073, respectively. The EXAFS analysis further reveals that Au was predominantly coordinated with Cl in Au/NC-413, and to N and/or O in Au/NC-973 and Au/NC-1073 (Figure 2e and Figure S6). The best fitting of the first shell reveals a coordination number (CN) of 2.0 for Cl, and 3.5 and 2.7, respectively, for N/O in the two high-temperature samples (Figure S6 and Table S4). This change in Au coordination atoms from Cl to N/O upon high-temperature activation is fully supported by surface elemental concentrations determined by XPS, as the substantial amount of Cl in the low-temperature samples (Cl:Au > 37, molar ratio) was almost completely removed after treatment at $T \geq$ 973 K, but the N content remains rather stable (Figure S7 and Table S3).

The remarkable stabilization of single Au atom on the NC carrier was rationalized by density functional theory (DFT). The most representative coordination environments were determined (Figure 2f) by analyzing the intrinsic stability (Tables S6, S7 and Figure S8), the ability to bind Au or AuCl, and the barriers for diffusion of gold species from the cavity to the host surface of several nitrogen defects. The analysis of formation energy (E) of an isolated AuCl molecule on multiple cavities reveals that NC-Au-Cl moiety is thermodynamically stable on diverse structures. Since at low temperatures relatively high amounts of Cl are present, in Au/NC-413 the photosensitive NC-Au-Cl species (from **b1** to **b6,** Figure 2f) are likely displayed as Au^0 (**a1**, E = −1.48 eV) by XPS analysis (vide supra). Upon increasing the temperature, the removal of Cl in combination with the higher mobility of Au atoms leads to the emergence of the Au^+ feature at 573 K corresponding to the oxidized-4-pyridinic structure (**a4**, E = −1.71 eV). The calculated Au 4f XPS shift is much higher than that experimentally observed (1.74 vs. 0.80 eV), indicating likely $Au^{\delta+}$ ($1 < \delta < 3$) species in **a4**. A further temperature increase involves higher diffusion of gold species that enter the **a6** cavity adopting a four-fold N-coordinated planar geometry, which represents the global diffusion minima (E = −3.61 eV) and is observed as Au^{3+} by XPS and EXAFS.
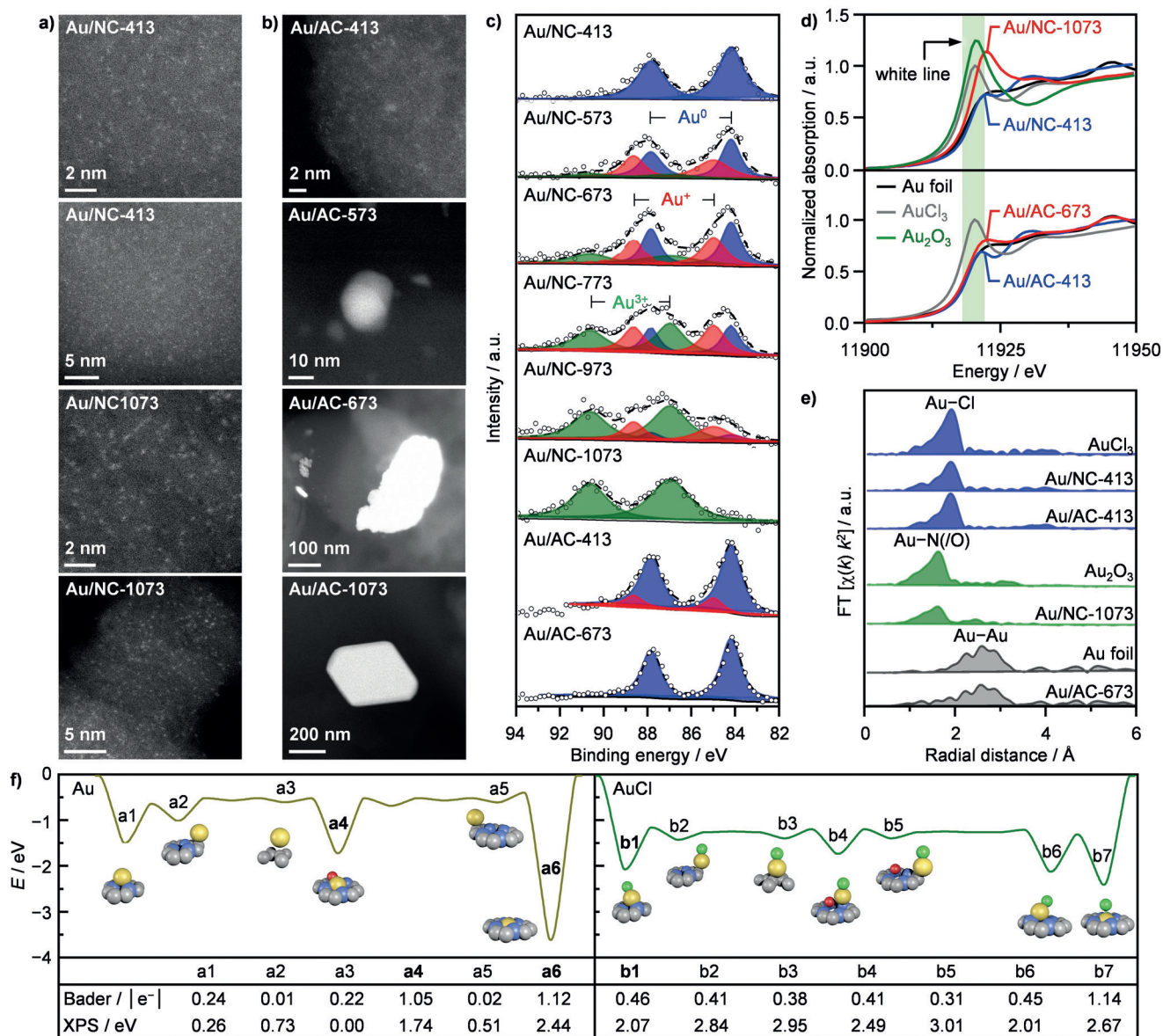
Figure 2. a) Aberration corrected HAADF-STEM micrographs of Au/NC-*T* and b) HAADF-STEM images of Au/AC-*T* catalysts, presenting the comparative evolution of gold atoms on the two carriers. c) Au 4f core level XPS spectra and, d) ex situ Au *L*₃ edge-normalized XANES spectra together with e) the FT-EXAFS spectra of key gold catalysts and reference samples. f) Energy profiles for the surface diffusion of Au and AuCl between 3-pyridinic, graphite, oxidized-4-pyridinic and 4-pyridinic, with the Bader charges and Au 4f XPS shifts (relative to an Au atom on the graphite basal plane, Au yellow, C gray, N blue, O red, Cl green) presented in the bottom panel. The most representative gold species are highlighted in bold.

The performance of the nanostructured gold catalysts (Au/NC-*T* and Au/AC-*T*) was evaluated in the continuous flow three-phase semi-hydrogenation of 1-hexyne and 2-methyl-3-butyn-2-ol (Figure 3a and Figure S9), two relevant reactions in the production of α-olefins and synthesis of intermediate for vitamins.[13] The single-atom catalyst Au/AC-413 shows approximately three-fold higher activity than the rest Au/AC samples containing mainly Au nanoparticles. On the other hand, the two substrates display strikingly different catalytic responses on the Au/NC-*T* series. While the 1-hexyne hydrogenation activity is independent on the activation temperature and consequent Au speciation, a volcano-like curve is observed in the case of 2-methyl-3-butyn-2-ol. In accordance with the literature reports,[14] all these gold systems give essentially full selectivity to the aimed alkenes. In addition, HAADF-STEM examination on the two extreme Au/NC-*T* catalysts confirmed that the atomic dispersion of gold remains unaltered after the hydrogenation performance (Figure S10).

To gain confidence on the above catalytic phenomenon on Au/NC-*T*, we then extend the substrate scope (Figure 3b and Figure S9). The experimental results show that irrespective of the chain length (1-dodecyne) and the position of the C≡C bond (4-octyne), the hydrogenation of unfunctionalized substrates does not show any dependence on the gold coordination sphere and speciation. Consistently, all adsorp-
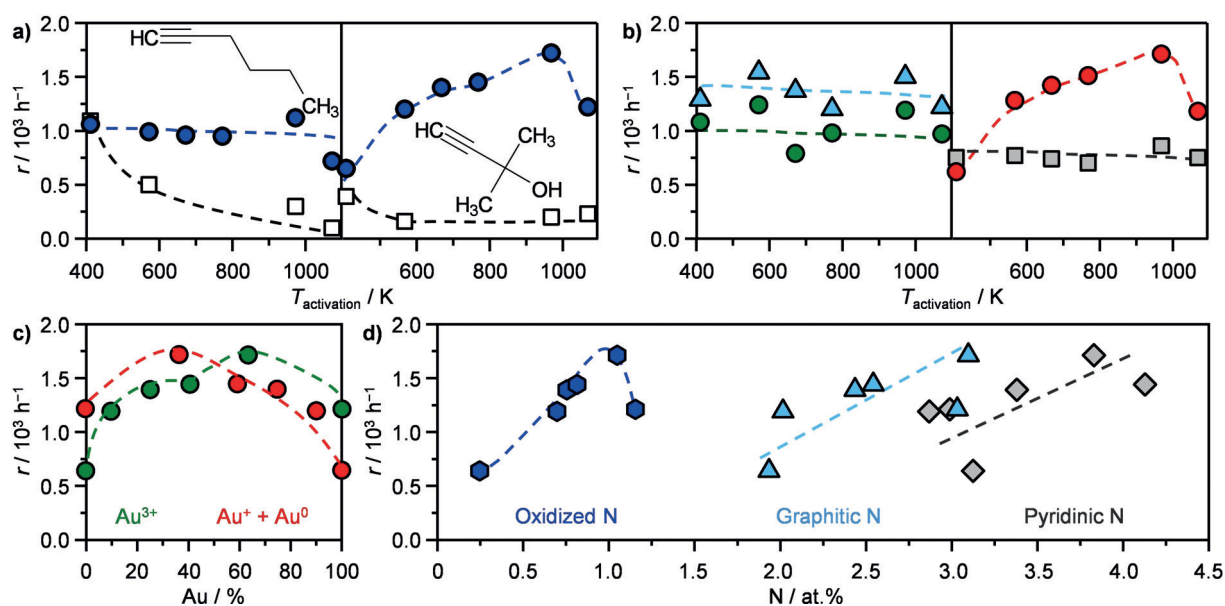
Figure 3. a) Comparative performance of Au/NC-*T* (circle) and Au/AC-*T* (square) catalysts in 1-hexyne and 2-methyl-3-butyn-2-ol semi-hydrogenation. b) Extrapolation of the substrate specificity to 1-dodecyne (light blue), 4-octyne (green), 3-methyl-1-pentyl-3-ol (red), and 4-pentyl-1-ol (gray) over Au/NC-*T*. Reaction rate as a function of c) the Au oxidation state, based on the XPS fitting, and d) the nitrogen speciation. Conditions: $W_{cat} = 0.1$ g, $T = 303$ K, $P = 3$ bar, F_L(alkyne + toluene) = 1 cm³ min⁻¹, and F_G(H₂) = 48 cm³ min⁻¹. The alkyne conversion levels are around 5–25% under typical reaction conditions on all the catalysts evaluated.

tion energies of acetylene and 1-hexyne on relevant Au species are within a narrow range (from −0.18 to −0.53 eV; Figure 4 a), hinting that the molecules are bound in a similar manner. As evidenced in Figure S11, the slight difference in adsorption of the different substrates is due to the van der Waals contributions arising from the different numbers of the carbon atoms. Conversely, the reaction rate of 3-methyl-1-pentyl-3-ol hydrogenation presents volcano behavior similar to 2-methyl-3-butyn-2-ol, while the γ-alcohol 4-pentyl-1-ol behaves like the other unfunctionalized alkynes showing structure insensitivity. Therefore, this molecular recognition pattern[15] can be employed to identify the nature of the active site in terms of Au oxidation state and cavity functionaliza-

tion. From the reactant adsorption heatmaps we have identified that the most active site appearing at medium temperatures (773–973 K) is **a4**, which contains the oxidized-4-pyridine cavity and the Au$^{\delta+}$ species. Neither Au⁺ nor Au³⁺ alone are activity descriptor for the hydrogenation, while (oxidized) pyridinic N shows good correlation (Figures 3 c,d), supporting the above conclusion. The Au@**a4** ensemble ensures that the adsorption of different alkynols (Figure 4 a) is maximal for the α-ol due to the formation of a hydrogen bond, which is by far the largest adsorption obtained among all the alkynes studied (Figure S12). The reaction mechanism was then simulated on this specific site and consists of molecular hydrogen splitting by gold and the concomitant
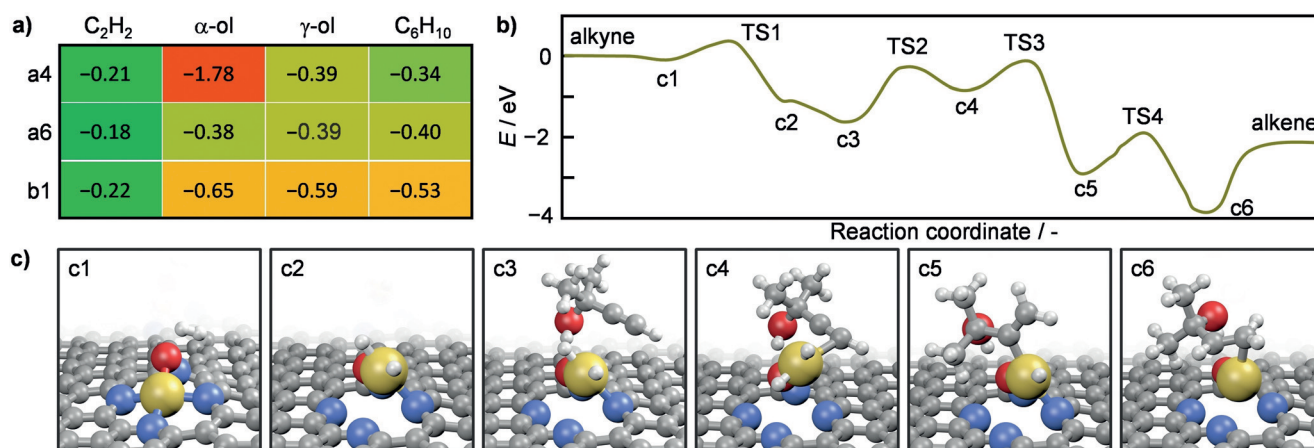

Figure 4. a) Heatmap for the adsorption of acetylene (C₂H₂), 2-methyl-3-butyn-2-ol (α-alcohol, α-ol), 4-pentyl-1-ol (γ-alcohol, γ-ol) and 1-hexyne (C₆H₁₀), and b) energy profile for the hydrogenation reaction of 2-methyl-3-butyn-2-ol on a single gold atom in the oxidized-4-pyridinic cavity. c) Side view of DFT-optimized adsorption configuration of the intermediates for the reaction profile in (b).

adsorption of 2-methyl-3-butyn-2-ol to the metal center and the N−O termination (Figure 4b and Video S1). Then, the two activated H are sequentially added to the triple bond, forming the alkene that detaches from the material. To rationalize the higher activity of Au single atoms over the nanoparticle analogues, we have computed the full reaction profile of 2-methyl-3-butyn-2-ol on the Au(211) surface (Figure S13). By comparing the H_2 activation step, the rate-determining step for Au-based catalysts,[9b] between Au@4 and Au(211), it is evidenced that the activation is significantly more thermodynamically favored on the single-atom sites than on the Au surface (-1.13 eV and -0.17 eV, respectively). Thus, the population of activated H is much higher on the single-atom catalyst to further continue the reaction. Besides, the **a4** site occupied by gold is also stable against hydrogen reduction (barrier 1.71 eV, Figure S14), that ensures the high stability of the hydrogenation performance as evidenced by HAADF-STEM of the used catalysts (see above).

In conclusion, we have developed an effective method to entrap single Au atoms with N-doped carbon, and demonstrated how to finely tailor their nature (oxidation state and coordination sphere) by taking advantage of their different thermal stability in the cavities of the host. Assessment of the diverse nanostructured gold catalysts in alkyne semi-hydrogenation confirms the higher activity of Au single atoms than nanoparticles. Furthermore, the hydrogenation over the single-atom Au/NC-*T* catalysts shows structure insensitivity for unfunctionalized alkynes and alkynols with γ-OH respect to the triple bond, and structure sensitivity for alkynols with α-OH. Theoretical methods link this unprecedented sensitivity behavior to the strong interactions between the adsorbed alkynol molecules and the gold and oxidized-4-pyridinic N ensemble, resulting in specific molecular recognition pattern in alkyne semi-hydrogenation. Overall, the precise control of the anchoring sites of single metal atoms developed in this study represents a key step towards the rational catalyst design, providing a novel way for breaking linear scaling relations that can be extrapolated to other hydrogenations and beyond.

Acknowledgements

Conflict of interest

The authors declare no conflict of interest.

[1] R. Dorel, A. M. Echavarren, *Chem. Rev.* **2015**, *115*, 9028 – 9072.

[2] a) M. Flytzani-Stephanopoulos, *Acc. Chem. Res.* **2014**, *47*, 783 – 792; b) M. Yang, S. Li, Y. Wang, J. A. Herron, Y. Xu, L. F. Allard, S. Lee, J. Huang, M. Mavrikakis, M. Flytzani-Stephanopoulos, *Science* **2014**, *346*, 1498 – 1501; c) X. F. Yang, A. Q. Wang, B. T. Qiao, J. Li, J. Y. Liu, T. Zhang, *Acc. Chem. Res.* **2013**, *46*, 1740 – 1748.

[3] a) Z. Chen, S. Pronkin, T.-P. Fellinger, K. Kailasam, G. Vilé, D. Albani, F. Krumeich, R. Leary, J. Barnard, J. M. Thomas, J. Pérez-Ramírez, M. Antonietti, D. Dontsova, *ACS Nano* **2016**, *10*, 3166 – 3175; b) N. Cheng, S. Stambula, D. Wang, M. N. Banis, J. Liu, A. Riese, B. Xiao, R. Li, T. K. Sham, L. M. Liu, G. A. Botton, X. Sun, *Nat. Commun.* **2016**, *7*, 13638; c) Y. J. Chen, S. F. Ji, Y. G. Wang, J. C. Dong, W. X. Chen, Z. Li, R. A. Shen, L. R. Zheng, Z. B. Zhuang, D. S. Wang, Y. D. Li, *Angew. Chem. Int. Ed.* **2017**, *56*, 6937 – 6941; *Angew. Chem.* **2017**, *129*, 7041 – 7045.

[4] a) G. Vilé, D. Albani, M. Nachtegaal, Z. Chen, D. Dontsova, M. Antonietti, N. López, J. Pérez-Ramírez, *Angew. Chem. Int. Ed.* **2015**, *54*, 11265 – 11269; *Angew. Chem.* **2015**, *127*, 11417 – 11422; b) D. A. Bulushev, M. Zacharska, E. V. Shlyakhova, A. L. Chuvilin, Y. N. Guo, S. Beloshapkin, A. V. Okotrub, L. G. Bulusheva, *ACS Catal.* **2016**, *6*, 681 – 691; c) P. Q. Yin, T. Yao, Y. Wu, L. R. Zheng, Y. Lin, W. Liu, H. X. Ju, J. F. Zhu, X. Hong, Z. X. Deng, G. Zhou, S. Q. Wei, Y. D. Li, *Angew. Chem. Int. Ed.* **2016**, *55*, 10800 – 10805; *Angew. Chem.* **2016**, *128*, 10958 – 10963.

[5] a) A. S. K. Hashmi, G. J. Hutchings, *Angew. Chem. Int. Ed.* **2006**, *45*, 7896 – 7936; *Angew. Chem.* **2006**, *118*, 8064 – 8105; b) A. M. Asiri, A. S. K. Hashmi, *Chem. Soc. Rev.* **2016**, *45*, 4471 – 4503.

[6] a) N. Masoud, L. Delannoy, H. Schaink, A. van der Eerden, J. W. de Rijk, T. A. G. Silva, D. Banerjee, J. D. Meeldijk, K. P. de Jong, C. Louis, P. E. de Jongh, *ACS Catal.* **2017**, *7*, 5594 – 5603; b) A. Hugon, L. Delannoy, C. Louis, *Gold Bull.* **2008**, *41*, 127 – 138.

[7] a) B. T. Qiao, J. X. Liu, Y. G. Wang, Q. Q. Lin, X. Y. Liu, A. Q. Wang, J. Li, T. Zhang, J. Y. Liu, *ACS Catal.* **2015**, *5*, 6249 – 6254; b) Z. Chen, Q. Zhang, W. X. Chen, J. C. Dong, H. R. Yao, X. B. Zhang, X. J. Tong, D. S. Wang, Q. Peng, C. Chen, W. He, Y. D. Li, *Adv. Mater.* **2018**, *30*, 8.

[8] G. Malta, S. A. Kondrat, J. S. Freakley, C. J. Davies, L. Lu, S. Dawson, A. Thetford, E. K. Gibson, D. J. Morgan, W. Jones, P. P. Wells, P. Johnston, C. R. A. Catlow, C. J. Kiely, G. J. Hutchings, *Science* **2017**, *355*, 1399 – 1403.

[9] a) M. García-Mota, N. Cabello, F. Maseras, A. M. Echavarren, J. Pérez-Ramírez, N. López, *ChemPhysChem* **2008**, *9*, 1624 – 1629; b) Y. Segura, N. López, J. Pérez-Ramírez, *J. Catal.* **2007**, *247*, 383 – 386.

[10] R. Lin, S. K. Kaiser, R. Hauert, J. Pérez-Ramírez, *ACS Catal.* **2018**, *8*, 1114 – 1121.

[11] Y. Y. Fong, B. R. Visser, J. R. Gascooke, B. C. Cowie, L. Thomsen, G. F. Metha, M. A. Buntine, H. H. Harris, *Langmuir* **2011**, *27*, 8099 – 8104.

[12] F. W. Lytle, P. S. P. Wei, R. B. Greegor, G. H. Via, J. H. Sinfelt, *J. Chem. Phys.* **1979**, *70*, 4849 – 4855.

[13] a) C. Moreno-Marrodan, F. Liguori, P. Barbaro, *Beilstein J. Org. Chem.* **2017**, *13*, 734 – 754; b) J. A. Delgado, O. Benkirane, C. Claver, D. Curulla-Ferré, C. Godard, *Dalton Trans.* **2017**, *46*, 12381 – 12403; c) M. Eggersdorfer, D. Laudert, U. Létinois, T.

McClymont, J. Medlock, T. Netscher, W. Bonrath, *Angew. Chem. Int. Ed.* **2012**, *51*, 12960 – 12990; *Angew. Chem.* **2012**, *124*, 13134 – 13165.

[14] J. L. Fiorio, N. López, L. M. Rossi, *ACS Catal.* **2017**, *7*, 2973 – 2980; J. L. Fiorio, R. V. Gonçalves, E. Teixeira-Neto, M. A. Ortuño, N. López, L. M. Rossi, *ACS Catal.* **2018**, *8*, 3516 – 3524.

[15] "Molecular Recognition": J. Lehn in *Supramolecular Chemistry* (Ed.: J. Lehn), Wiley, New York, **1995**, https://doi.org/10.1002/3527607439.ch2.